AGU PUBLICATIONS

Geophysical Research Letters

RESEARCH LETTER
10.1002/2016GL071930

Key Points:
- Calculated CH_4 radiative forcing is about 25% higher than earlier estimates
- New simplified expressions for forcing are presented for CO_2, N_2O, and CH_4
- Forcing for high CO_2 concentrations is 9% higher than previous expressions

Supporting Information:
- Supporting Information S1

Correspondence to:
K. P. Shine,
k.p.shine@reading.ac.uk

Citation:
Etminan, M., G. Myhre, E. J. Highwood, and K. P. Shine (2016), Radiative forcing of carbon dioxide, methane, and nitrous oxide: A significant revision of the methane radiative forcing, *Geophys. Res. Lett.*, *43*, 12,614–12,623, doi:10.1002/2016GL071930.

Received 22 APR 2016
Accepted 28 NOV 2016
Published online 27 DEC 2016

Radiative forcing of carbon dioxide, methane, and nitrous oxide: A significant revision of the methane radiative forcing

M. Etminan[1], G. Myhre[2], E. J. Highwood[1], and K. P. Shine[1]

[1]Department of Meteorology, University of Reading, Reading, UK, [2]CICERO Center for International Climate and Environmental Research, Oslo, Norway

Abstract New calculations of the radiative forcing (RF) are presented for the three main well-mixed greenhouse gases, methane, nitrous oxide, and carbon dioxide. Methane's RF is particularly impacted because of the inclusion of the shortwave forcing; the 1750–2011 RF is about 25% higher (increasing from 0.48 $W m^{-2}$ to 0.61 $W m^{-2}$) compared to the value in the Intergovernmental Panel on Climate Change (IPCC) 2013 assessment; the 100 year global warming potential is 14% higher than the IPCC value. We present new simplified expressions to calculate RF. Unlike previous expressions used by IPCC, the new ones include the overlap between CO_2 and N_2O; for N_2O forcing, the CO_2 overlap can be as important as the CH_4 overlap. The 1750–2011 CO_2 RF is within 1% of IPCC's value but is about 10% higher when CO_2 amounts reach 2000 ppm, a value projected to be possible under the extended RCP8.5 scenario.

1. Introduction

The radiative forcing (RF) due to changes in concentrations of the relatively well mixed greenhouse gases (WMGHGs) is the largest component of total RF due to human activity over the past century [*Myhre et al.*, 2013a].

The headline RF values for CO_2, CH_4, and N_2O presented in recent Intergovernmental Panel on Climate Change (IPCC) assessments [e.g., *Myhre et al.*, 2013a] are calculated using simplified expressions presented in the IPCC Third Assessment Report [*Ramaswamy et al.*, 2001, section 6.3.5]. These were largely based on the work of *Myhre et al.* [1998, henceforth MHSS98]. MHSS98 used updated RF calculations to modify expressions adopted by IPCC in its first assessment [*Shine et al.*, 1990] which originated from earlier work of *Hansen et al.* [1988] and *Wigley* [1987]. The MHSS98 expressions have been widely used elsewhere, for example, for calculating WMGHG RF in simple climate models and in NOAA's Annual Greenhouse Gas Index (http://www.esrl.noaa.gov/gmd/aggi/aggi.html (accessed 11 November 2016)). Other similar simplified expressions have been proposed [e.g., *Shi*, 1992; *Byrne and Goldblatt*, 2014], and *Hansen et al.* [2000] presented updates to the *Hansen et al.* [1988] fits.

The purpose of this letter is to update these expressions in a number of important ways. MHSS98 used broadband and narrowband radiation transfer calculations, which had been evaluated against clear-sky line-by-line (LBL) calculations, as a basis for the simplified expressions. Here all-sky LBL calculations are used directly. Since MHSS98, there have been many updates to spectroscopic data (both spectral lines and continua) which need to be incorporated. In addition, MHSS98 incorporated the shortwave component of the CO_2 RF; more recently, the potential importance of the shortwave bands of CH_4 has started to be recognized [*Collins et al.*, 2006; *Li et al.*, 2010] and we demonstrate the significance of these bands for RF here. The fits are also extended to cover a wider range of concentrations, including those relevant to the glacial-interglacial cycles over the past 800,000 years. Finally, we now incorporate the effect of the CO_2-N_2O spectral overlap [see, e.g., *Byrne and Goldblatt*, 2014] which was not included in MHSS98.

Byrne and Goldblatt [2014] have also presented simplified expressions based on high-spectral-resolution calculations, but there are restrictions in using their expressions. First, they reported instantaneous forcings (see *Myhre et al.* [2013a] for detailed definitions) and so neglected the role of stratospheric temperature adjustment on RF (see below). Second, the form of their expressions (which are referenced to preindustrial concentrations) means that they are less easy to apply to arbitrary changes in WMGHG concentrations over their range of applicability. They do, however, extend to a wider range of concentrations, making them potentially applicable to gas concentrations several million years ago.

The RF calculations here include adjustment to stratospheric temperatures, which is known to improve the utility of RF as a predictor of surface temperature change in climate models, compared to the instantaneous forcing [e.g., *Myhre et al*., 2013a]. *Myhre et al*. [2013a] presented the concept of effective radiative forcing (ERF), which includes tropospheric adjustments (of, for example, temperatures and clouds) with surface temperatures held fixed. ERF is a conceptually more applicable predictor of surface temperature response across a wide range of forcing mechanisms. However, it would be a formidable job to calculate ERFs for the range of cases presented here; it would require the use of climate models, with low-spectral-resolution radiative transfer codes, and the tropospheric adjustment would likely be significantly model dependent. *Myhre et al*. [2013a] concluded that the central estimates of ERFs for the WMGHGs considered here were the same as the stratosphere-adjusted RFs, but with a larger uncertainty. Unlike MHSS98, we do not include RF due to halogenated gases, as these have been covered in detail by *Hodnebrog et al*. [2013].

2. Methods

The RF calculations use the Oslo line-by-line (OLBL) code which was described in *Myhre et al*. [2006]. OLBL has contributed, as a benchmark model, to several radiation code intercomparisons including *Forster et al*. [2005, 2011], *Myhre et al*. [2009], and *Randles et al*. [2013]. We use the *Myhre et al*. [2006] two-atmosphere (tropical/extratropical) approach, which includes cloud data from the International Satellite Cloud Climatology Project, to generate global forcings. OLBL code is based on the GENLN2 LBL code, which was used to generate the clear-sky forcings presented in MHSS98, but it has been enhanced in a number of important ways. It is coupled to a 16-stream Discrete Ordinate code [*Stamnes et al*., 1988] to compute irradiances and now includes clouds and stratospheric temperature adjustment using the standard fixed-dynamical heating methodology. The shortwave RF part of OLBL is now updated to be representative for global simulations. The solar irradiance spectrum is taken from *Lean et al*. [2005]. Solar radiative transfer simulations are performed for five solar zenith angles, and day length fraction is calculated for the tropical and extratropical profiles. Present-day natural and anthropogenic aerosols are included using the OsloCTM2 simulations for AeroCom Phase II [*Myhre et al*., 2013b] with broadband surface albedos taken from the same simulations. Absorption data from HITRAN 2008 edition [*Rothman et al*., 2009] are adopted both for the longwave and shortwave RF calculations. During this work the water vapor continuum was also updated (see section 3.2 for details).

We use 48 combinations (see supporting information Table S1) of CO_2, N_2O, and CH_4 concentrations covering the range from the lowest typical values in the 800,000 year ice core record (180 ppm of CO_2, 200 ppb of N_2O, and 340 ppb of CH_4) [*Masson-Delmotte et al*., 2013] to the highest anticipated amount in the year 2300 (2000 ppm of CO_2, 525 ppb of N_2O, and 3500 ppb of CH_4) [*Meinshausen et al*., 2011].

3. Radiative Forcing Calculations

3.1. Results

The RF results for all 48 cases are presented in Table S1 and include the shortwave RF, the instantaneous clear-sky and all-sky longwave RF, the adjusted longwave RF (which includes the influence of the shortwave forcing on stratospheric temperature), and the net forcing. The row numbers in Table S1 will be used to refer to particular cases; forcing values for the cases where only one gas changes, and the impact of overlap, are shown in Figure 2, which will be discussed in section 4. The change, relative to the MHSS98 expressions, is also shown in Table S1. Updated expressions are discussed in section 4. The new calculations are, for the most part, within about 5% of the old fits, but with a few notable exceptions. In particular, for cases where only methane changes (Table S1, rows 4, 7, and 10), the new calculations are 17–27% higher than the old fits—the reasons for this will be discussed in section 3.2. For high CO_2 cases (2000 ppm—Table S1, rows 37–48) the new calculations are typically 10% higher than the old fits, indicating that the CO_2 forcing increases more rapidly than expected from a purely logarithmic dependence (as noted by others [e.g., *Hansen et al*., 1988; *Zhong and Haigh*, 2013], and see section 4). Such high CO_2 amounts were outside the range considered by MHSS98. The ice age CO_2 concentrations (180 ppm—Table S1, rows 13–24) were also outside the range considered in MHSS98, but nevertheless, the old fits are within about 5% of the new calculations, which indicates that the pure logarithmic dependence was more appropriate for lower CO_2 levels. A few cases in Table S1

(rows 6, 8, and 12) have a high error (exceeding 50%) where the forcing is a small residual due to an increase in CH_4 and a decrease in N_2O, or vice versa.

3.2. Explanation of Methane Forcing Changes

The most striking feature of the results is the enhancement of the methane RF by about 17–27% compared to the old expressions; this is beyond the nominal uncertainty estimates (about 10%) given in successive IPCC reports for WMGHG forcings. Two mechanisms are responsible–it is primarily due to the role of methane's shortwave bands, which were not included in MHSS98, with a secondary effect of an update to the water vapor continuum strength relative to that used in MHSS98.

Considering, as an example, the CH_4 change, from 750 to 1800 ppb (Table S1, row 4), the instantaneous shortwave forcing due to methane (0.03 $W m^{-2}$) is about 6% of the total methane forcing (0.58 $W m^{-2}$). This is further enhanced because the shortwave forcing affects stratospheric temperature adjustment; this effect is manifested by the change between the instantaneous and adjusted longwave forcings. Without the shortwave effect, the adjustment is found to be small and negative; the instantaneous RF of 0.516 $W m^{-2}$ decreases by 2% to 0.504 $W m^{-2}$ after adjustment for the 750–1800 ppb CH_4 change. *Rind and Lacis* [1993] report a 0.5% decrease after stratosphere temperature adjustment for a 280–560 ppb change in CH_4, using a radiative-convective model. When methane's shortwave absorption is included, the longwave adjustment is *positive*, increasing the longwave forcing from its instantaneous RF value of 0.516 to 0.548 $W m^{-2}$ after adjustment, a 6% increase (or 9% relative to adjusted forcing without the shortwave effect). Hence, in total, the shortwave effect increases the methane forcing by 15% from its adjusted longwave-only value of 0.504 to 0.582 $W m^{-2}$.

The fact that the shortwave forcing for CH_4 is positive is notable, in the context of earlier work. For CO_2, the shortwave bands cause a forcing that opposes and so acts to decrease the magnitude of the CO_2 longwave-only forcing by about 5% (e.g., MHSS98 and Table S1, rows 13, 25, and 37); this is due to the combined effect of the direct absorption of the solar radiation in the stratosphere and its subsequent effect on temperature adjustment. For CH_4, the instantaneous forcing calculations of *Collins et al*. [2006] and *Forster et al*. [2011] also imply a negative, rather than a positive shortwave forcing; in *Collins et al*. [2006] the shortwave forcing is 15% of, but the opposite sign to, the longwave irradiance change at 200 hPa for a doubling of CH_4 from preindustrial concentrations. However, these calculations were for an idealized clear-sky case with a fixed solar zenith angle of 53° and a surface albedo of 0.1. The shortwave bands of N_2O contribute less than 1% of the forcing; this forcing is included here but discussed no further.

The contrasting signs of the shortwave forcings of CH_4 and CO_2 can be explained by reference to Figure 1. This shows the spectral variation of global-mean shortwave net forcing for the two gases (180 ppm to 389 ppm for CO_2 and 750 to 1800 ppb for CH_4). Supporting information Figure S1 shows the upward and downward forcing components. For both gases (Figures 1a and 1b), the sign of the forcing varies with wavelength, the net impact being the residual of these. In the case of CO_2 the negative forcing due to its 2.7 μm band dominates. For CH_4, the positive forcing due to its 1.7 and 2.3 μm bands dominates. This contrasting behavior is driven by two processes. One is the stratospheric opacity of the gases, and the other is the degree of overlap of absorption bands with the near-IR bands of water vapor. Figures 1c and 1d show the sum of line strengths for each 1 nm interval in the OLBL for water vapor (in both plots) and CO_2 and CH_4.

For all bands, the downward shortwave flux at the tropopause is always decreased by the increased concentrations, due to increased absorption in the stratosphere (Figures S1a and S1b). The sign of the forcing depends on whether this negative contribution dominates over the increased absorption by these gases in the troposphere, which contributes a positive forcing. For CO_2, the extremely strong band at 4.3 μm makes little contribution to forcing at band center; absorption is almost complete in the stratosphere at unperturbed concentrations, and it only starts to contribute to forcing at the band edges. The CO_2 2.7 μm band lies toward the center of a strong water vapor band (Figure 1d). The change in the downward forcing is strongly negative (Figure S1b), but there is not a compensating increase in tropospheric absorption because the heavy spectral overlap with water vapor strongly mutes the impact of CO_2 increases. By contrast, the weaker bands of CO_2 at 1.6 and 2.0 μm lie in, or toward the edges of, windows between the main water vapor bands (Figure 1d); hence, they are more able to increase tropospheric absorption causing a positive forcing that dominates over the negative stratospheric component.

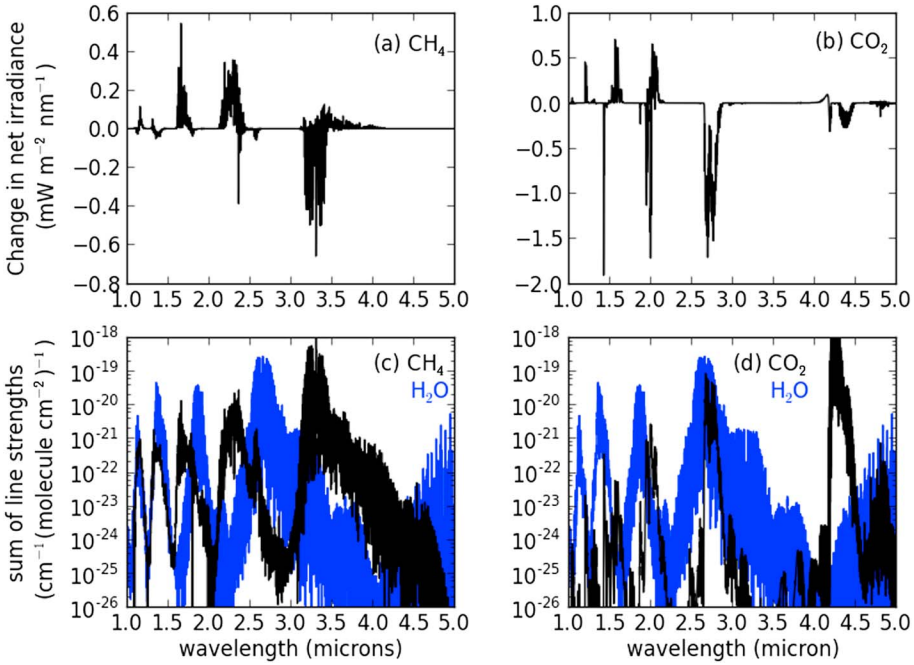

Figure 1. Spectral variation of near-infrared tropopause forcing (global-mean, all sky) for (a) CH_4 (750 to 1800 ppb) and (b) CO_2 (180 to 389 ppm). The sum of the absorption line strengths in each 1 nm spectral interval is shown for (c) CH_4 and (d) CO_2, with H_2O line strengths shown in blue in both frames.

Methane has a strong band at 3.3 μm (Figure 1a), which lies within a region of relatively strong water vapor absorption (Figure 1c), leading to a negative net forcing. The weaker bands at 1.6 and 2.3 μm lie toward the center of the windows in the water vapor spectrum. They cause a positive forcing which more than compensates for the 3.3 μm negative forcing. In summary, the magnitude and sign of the solar RF depend on band strength, gas concentration, and overlap with water vapor.

The contrast with the implied negative forcing in earlier work originates from clouds. For the *Collins et al.* [2006] clear-sky case, there is little tropospheric upward scatter of radiation (no clouds and low surface albedo), so that photons largely take a single pass through the troposphere. When clouds are added, the added CH_4 absorbs not only downwelling radiation but also upward scattered radiation, greatly increasing the tropospheric absorption (see Table S2). For both the extratropical and tropical cases, the inclusion of clouds causes the shortwave RF to change from a negative to a positive forcing of almost the same size; the negative clear-sky forcing of about $-0.04\,W\,m^{-2}$ is consistent with the *Collins et al.* [2006] value of $-0.13\,W\,m^{-2}$ (for approximately the same methane change) after accounting for the higher incoming solar irradiance for their (fixed-Sun) case. The effect of clouds on the shortwave RF from CH_4 is similar to the effect of clouds on the shortwave RF of black carbon aerosols [*Haywood and Shine*, 1997].

In trying to reconcile the present (longwave) results with those in MHSS98, we identified a further influence on the forcing due to CH_4 (and, to a lesser extent, the N_2O). MHSS98 used the Clough-Kneizys-Davies (CKD) water vapor continuum version 0 in the OLBL calculations. In the region of the CH_4 and N_2O bands that are most responsible for the longwave forcing (around $1300\,cm^{-1}$), the foreign continuum was weakened by about a factor of 3.5 in subsequent versions of CKD [e.g., *Mlawer et al.*, 1998] and successor versions (the Mlawer-Tobin-CKD) [*Mlawer et al.*, 2012]. This reduces the effect of water vapor overlap with CH_4, increasing its RF. Changes in the self-continuum in this spectral region were much smaller during these updates. To isolate the effect of the continuum changes, the instantaneous cloudy-sky longwave forcings were examined when CKD version 0 is updated to version 2.4.1. The update caused the CH_4 forcing for a 1800 to 3500 ppb change to increase by 4.2%. For comparison, the N_2O forcing increased by about 1.7% for a 323 to 525 ppb change; for CO_2, RF changed by less than 0.2%.

In total, comparing the new RFs to those calculated with the MHSS98 expressions, the CH_4 forcing increases by 17–27% for cases 4, 7, and 10 shown in Table S1. This is mostly due to the shortwave forcing, with a smaller

contribution from the decreased strength of the foreign continuum in the region of methane's longwave bands. We note that contemporary radiation codes used in climate models often neglect the shortwave band of methane (e.g., all those models participating in the *Collins et al*. [2006] and CCMval [*Fomichev and Forster*, 2010] intercomparisons); by contrast, it is likely that more recent versions of the water vapor continuum in the mid-infrared are already in use in these codes, and so they will be less affected by this component of our update to the MHSS98 calculations.

Based on our findings, the neglect of the CH_4 shortwave bands would underestimate the total historical anthropogenic RF by about 0.1 W m^{-2} and hence underestimate temperature change. However, many climate models have too high longwave RF of methane, which could (inadvertently) compensate, to some extent, for the lack of solar absorption by methane [*Collins et al*., 2006]. The same is true for models in the CCMval comparison [*Fomichev and Forster*, 2010], where the majority of model configurations gave too high a methane longwave forcing, some by as much as 30% (E. Rozanov, personal communication, 2016). Solar absorption by methane has not been included in observationally based estimates of climate sensitivity [e.g., *Skeie et al*., 2014; *Johansson et al*., 2015], and thus, these have used a too low total historical RF; however, the change in methane RF is relatively small compared to uncertainties in many of the non-greenhouse gas RFs and in particular those related to aerosol RF. Finally, we note that the strong spectral variation of the sign of the CH_4 forcing (Figure 1), and its strong dependence on the overlap with water vapor, may pose a challenge to its accurate representation in climate model radiation codes, with relatively low spectral resolution.

3.3. CO_2-N_2O Overlaps

Nitrous oxide possesses a moderately strong band centered at 17 μm, which overlaps with the high-wavelength side of the 15 μm complex of CO_2 absorption bands; hence, N_2O forcing can be affected by CO_2 changes and vice versa. This overlap was neglected in most previous simplified expressions of CO_2 [e.g., *Shi*, 1992; *Hansen et al*.,1988; MHSS98; *Ramaswamy et al*., 2001]. It was included (but not highlighted) in *Byrne and Goldblatt's* [2014] calculations of cloudy-sky instantaneous RF.

As shown in Table S1, the N_2O forcing for a change from 200 to 525 ppb is diminished by about 14% when using a CO_2 value of 2000 ppm (0.83 W m^{-2}, differencing rows 38 and 39) rather than 180 ppm (0.97 W m^{-2}, differencing rows 14 and 15), assuming CH_4 at 1800 ppb. This is almost the same as the effect on N_2O RF but using a CH_4 value of 3500 ppb (0.89 W m^{-2}, differencing rows 11 and 12) rather than 340 ppb (1.02 W m^{-2}, differencing rows 8 and 9), assuming CO_2 at 389 ppm. Hence, when calculating the N_2O forcing, coincident changes in CO_2 can be as important as coincident changes in CH_4.

The CO_2 forcing for a 180 to 2000 ppm change is diminished by about 1% if N_2O values of 525 ppb (differencing rows 15 and 39) are used, rather than 200 ppb (differencing rows 14 and 38), assuming CH_4 at 1800 ppb. By contrast, the CO_2 forcing changes by less than 0.1% across the range of CH_4 concentrations investigated here (for example, differencing rows 46 and 19, versus rows 43 and 22).

3.4. Uncertainties

Successive IPCC assessments [see *Myhre et al*., 2013a, section 8.3.1] have drawn on a range of evidence to estimate an uncertainty range for the WMGHG RFs of ±10%, when calculated using line-by-line codes. *Hodnebrog et al*. [2013] (see especially their section 3.6) presented an extended discussion of sources of uncertainty in forcing, based on the prior literature, including intercomparison studies. Although this was in the context of halocarbon radiative forcing, much of the discussion carries over to the longwave component of the WMGHG RFs discussed here.

There are distinct sources of uncertainty, including the underlying spectroscopic data, the calculation methodology, and the specification of atmospheric conditions (and the averaging of these conditions). Assessment of the impact of the then recent updates of the HITRAN database on longwave forcing [e.g., *Kratz*, 2008], and a more detailed assessment specifically for CO_2 [*Mlynczak et al*., 2016], indicates uncertainties of less than 1%. *Hodnebrog et al*. [2013] estimate that uncertainties from the radiation code and the method of calculating stratospheric adjustment are 5 and 4%, respectively, while specification of atmospheric temperature, clouds, and tropopause position each contributes 3%, 5%, and 4%, respectively, and that due to temporal and spatial averaging is about 1%. Their overall conclusion was that the total (5–95%) uncertainty was ±13% for halogenated gases; this is slightly higher than the *Myhre et al*. [2013a]

estimate of 10% for all WMGHGs, but the increase is specific to the halocarbons where uncertainties in spectroscopic data and the vertical profile are higher than the gases considered here.

We are not aware of such a detailed assessment for WMGHG forcing in the shortwave. *Collins et al*. [2006] show good agreement among four line-by-line codes for the shortwave forcing of greenhouse gases, for a specified clear-sky atmospheric state, and a single zenith angle; for example, at 200 hPa, the standard deviation was about 2% of the mean for CO_2 and a water vapor perturbation and no more than 4% (given the precision that their results were reported) for CH_4. However, now that our calculations demonstrate an enhanced role for methane in this spectral region, a more detailed assessment becomes important. *Rothman et al*. [2013] note incomplete understanding of CH_4 line shapes particularly in the near-infrared; the impact of future HITRAN versions on calculations of the CH_4 shortwave forcing will need to be assessed. *Toon et al*. [2016] note a number of instances in this wavelength region where balloon-borne spectral measurements are in better agreement with versions of HITRAN prior to the 2012 edition. In addition, there is ongoing uncertainty in the strength of the water vapor continuum in near-IR windows, particularly at atmospheric temperatures, [e.g., *Shine et al*., 2016], where the CH_4 shortwave forcing is important (Figure 1).

Other error sources for computing shortwave forcing, beyond those considered for the longwave, include those resulting from the specification of surface albedo and aerosol concentrations and the integration over day length to produce a day-averaged forcing; these will also be affected by the temporal and spatial averaging used. A number of sensitivity tests of the solar forcing were performed here for CH_4 changes from 750 to 1800 ppb, with all other gases held fixed. The complete removal of aerosol reduces the shortwave forcing by 10%, as the lower albedo means less reflected solar radiation to be absorbed by CH_4. Similarly, increasing the surface albedo by 1 percentage point (from a global-mean value of 12.3 to 13.3%) increased the shortwave forcing by 6.7%. These sensitivity studies indicate that there is some interdependence between the CH_4 shortwave forcing and other forcings, which could be examined in more detail in future work. Increasing the number of solar zenith angles at which the forcing is calculated from 5 to 15 changed the forcing by only 0.2%.

We retain the *Myhre et al*. [2013a] ±10% uncertainty range for the longwave forcing and hence use this for the total uncertainty for CO_2 and N_2O, given the small contribution from the shortwave forcing for these gases. For CH_4 we tentatively adopt a shortwave forcing uncertainty of about double this value (±25%), but given that the shortwave forcing is about 15% of the total forcing (including its contribution to the longwave adjustment discussed in section 3.2), this yields a total uncertainty in CH_4 forcing of about ±14%.

4. Simplified Expressions

Based on the results presented in section 3, the MHSS98 simplified expressions are updated. While the basic forms of the equations are retained, important modifications are introduced, in order to achieve improved agreement with the detailed calculations, over the range of concentration changes. The new expressions, derived using polynomial fitting, are shown in Table 1 and are valid for the CO_2, N_2O, and CH_4 concentrations given in section 2.

For CO_2, the logarithmic form used in MHSS98 ($RF = \alpha \ln(C/C_o)$, where C_o and C are the initial and final CO_2 concentrations) is retained but the nature of α term is changed; instead of being a constant, it is now a function of the CO_2 and N_2O concentrations. Note that the absolute value of CO_2 concentration change $|C\text{-}C_o|$ is adopted in the α term, to ensure that the forcing is symmetric for increases or decreases in CO_2. That is, $RF(C, C_o) = -RF(C_o, C)$. The $C\text{-}C_o$ terms only become important for large changes in CO_2; as shown below, for historical forcings, ignoring these terms and using the simple $\alpha \ln(C/C_o)$ form, and a midrange N_2O concentration, yields a value of α within 1% of the value of 5.35 W m^{-2} given in MHSS98.

For N_2O and CH_4, the basic square root dependence of RF used in MHSS98 (e.g., for N_2O, $RF = \beta(\sqrt{N} - \sqrt{N_o})$ plus an overlap term) is retained, but with two changes: the β term is no longer a constant, and it also now incorporates the overlap terms. MHSS98 adopted the *Hansen et al*. [1988] overlap term; this had the useful feature that it was the same for both N_2O and CH_4, but it is a complicated expression including the logarithm of products of N_2O and CH_4 raised to noninteger powers. We find that a different approach, with separate N_2O and CH_4 overlap terms, enables the overlap to be included by modifying the β term. In addition, as noted in section 3, it is necessary to include a $N_2O\text{-}CO_2$ overlap term.

Table 1. Simplified Expressions for Radiative Forcing of CO_2, CH_4, and N_2O, Where C Is the CO_2 Concentration (in ppm), M Is the CH_4 Concentration (in ppb), and N Is the N_2O Concentration (in ppb)[a]

Gas	Simplified Expression	Coefficients	Maximum Absolute Error Relative to Line-by-Line Model % (Wm^{-2})
CO_2	$\left[a_1(C-C_0)^2+b_1\lvert C-C_0\rvert+c_1\overline{N}+5.36\right]\times\ln\left({}^{C}/_{C_0}\right)$	$a_1=-2.4\times10^{-7}Wm^{-2}ppm^{-1}$ $b_1=7.2\times10^{-4}Wm^{-2}ppm^{-1}$ $c_1=-2.1\times10^{-4}Wm^{-2}ppb^{-1}$	3.6 (0.15)
N_2O	$\left[a_2\overline{C}+b_2\overline{N}+c_2\overline{M}+0.117\right]\left(\sqrt{N}-\sqrt{N_0}\right)$	$a_2=-8.0\times10^{-6}Wm^{-2}ppm^{-1}$ $b_2=4.2\times10^{-6}Wm^{-2}ppb^{-1}$ $c_2=-4.9\times10^{-6}Wm^{-2}ppb^{-1}$	0.64 (0.003)
CH_4	$\left[a_3\overline{M}+b_3\overline{N}+0.043\right]\left(\sqrt{M}-\sqrt{M_0}\right)$	$a_3=-1.3\times10^{-6}Wm^{-2}ppb^{-1}$ $b_3=-8.2\times10^{-6}Wm^{-2}ppb^{-1}$	2.7 (0.016)

[a] C, M, and N are concentration at the time at which the forcing is required, and C_o, M_o, and N_o are the initial concentrations. For terms within the square brackets, the gas concentrations are the mean of the initial and final concentrations (e.g., $\overline{M}=0.5(M+M_o)$ for methane) when the concentrations of those overlapping gases are also changing. The expressions are valid in the ranges 180–2000 ppm for CO_2, 200–525 ppb for N_2O, and 340–3500 ppb for CH_4. The maximum absolute error, relative to the OLBL (in % and, in parentheses, in Wm^{-2}), is shown in the final column. Note that the absolute uncertainty in the OLBL calculations is estimated to be 10% for CO_2 and N_2O and 14% for CH_4 (see section 3.4).

In all cases, the overlap term is treated differently to previous practice. In most previous work including MHSS98, the overlap term has been treated by considering the final concentration of the gas for which the RF is being calculated (e.g., M, in the case of CH_4) and the initial concentration of overlapping gas (e.g., N_o when calculating the CH_4 RF and M_o when calculating the N_2O RF). By contrast *Myhre et al.* [2013a] used the final concentrations of the overlapping gases (e.g., N when calculating CH_4 RF). One undesirable aspect of both approaches is that the calculated RF is not symmetric about increases and decreases in the gas concentration (e.g., $RF(M,M_o)\neq-RF(M_o,M)$) if the overlapping gas changes in concentration. To alleviate this problem, the mean concentration (e.g., $\overline{M}=0.5(M+M_o)$) is adopted here for all terms (other than the (C-C_o) terms) within the square brackets in Table 1 equations—the quality of the fits is, in the majority of cases, superior to using the final concentrations.

The final columns of Table S1 show the RF calculated using the new expressions, for each gas separately, and their sum, and the error in the sum relative to the OLBL calculations. Except for two cases where the CH_4 and N_2O forcings strongly oppose each other (Table S1, rows 6 and 8, and see section 3.1), the new expressions reproduce the OLBL forcings to within better than 5% across the range of concentration changes. In a few cases, the old fits are better, but the most severe cases (Table S1, rows 16, 18, and 24) are for unlikely combinations with very low paleo-CO_2 and present or future concentrations of N_2O. Even in the worst of these cases, the new fits reproduce the OLBL calculations to within better than 4%; however, taken as a whole, the new fits are considerably better.

The results are summarized in Figure 2. Figures 2a–2c show the individual forcings for CO_2, CH_4, and N_2O, comparing the new expressions with the OLBL results. Figure 2d illustrates the strength of the overlap terms, and their representation by the new expressions, by showing the difference in forcing for a given gas, between the highest and lowest concentrations of the overlapping gases; since this range covers the entire ice age to maximum projected 2300 values, it represents an extreme test. For CO_2 the difference in forcing between the maximum and minimum N_2O concentrations is at the 1% level, and for CH_4 the effect of N_2O overlap is at less than the 10% level. For N_2O, both CO_2 and CH_4 overlaps contribute about equally, for the specified concentration changes, with the difference exceeding 10% for each gas.

5. Impact on Historical and Future Forcings and Emission Metrics

The new expressions increase the IPCC AR5 [*Myhre et al.*, 2013a, Table 8.2] RFs for CO_2, CH_4, and N_2O for the period 1750–2011 from 1.82, 0.48, and 0.17 Wm^{-2} to 1.83, 0.61, and 0.17 Wm^{-2} or by 0.5%, 25%, and 2%, respectively; the difference in the sum of the three forcings is 0.14 Wm^{-2}. Provisional values for 2015 global-annual-mean concentrations (from http://www.esrl.noaa.gov/gmd/—accessed 3 October 2016) for CO_2 (399 ppm), CH_4 (1834 ppb), and N_2O (328 ppb) (using the same preindustrial values of 278 ppm, 722 ppb,

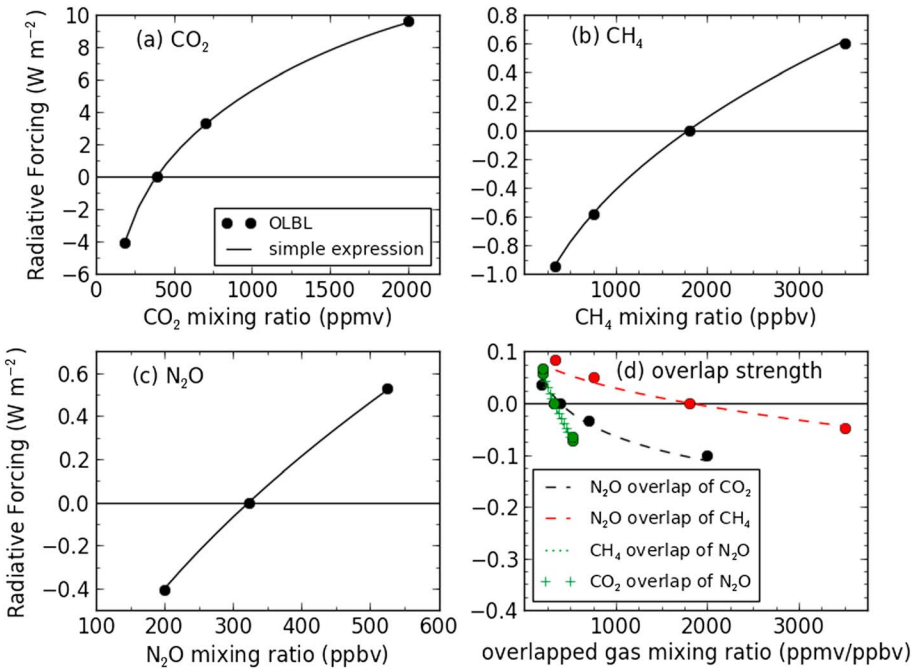

Figure 2. Comparison of OLBL radiative forcing with the new simple expressions for (a) CO_2, (b) CH_4, and (c) N_2O. The forcings are relative to 389 ppm for CO_2, 1800 ppb for CH_4, and 323 ppb for N_2O; the effect of overlapping gases is included using these same mixing ratios. (d) Illustration of the effect of the overlap on forcings for OLBL (symbols) and simple expressions (lines); the difference between the forcing for the highest and lowest concentrations of the overlapping gas is plotted: N_2O overlap (525 minus 200 ppb), CH_4 overlap (3500 minus 340 ppb), and CO_2 overlap (2000 minus 180 ppm). The effect of CH_4 and CO_2 overlaps of N_2O are almost the same for these choices of mixing ratio, so that these lines are almost coincident on the plot.

and 270 ppbv, respectively) yield RFs of 1.95, 0.62, and 0.18 W m^{-2}; this gives an increased RF for these three gases of 0.14 W m^{-2} relative to 2011 concentrations, using the new expressions.

Figure 3a compares the RF derived from old and updated expressions for 1750–2011; for the new expressions, the shaded area shows the radiative uncertainty discussed in section 3.4. It shows that for CO_2 the RF using the old and new expressions differs by only about 1%. As anticipated from the results in section 3, this difference is larger for the other two gases; in 2011 it is about 2% for N_2O forcing and 25% for CH_4 forcing.

Figure 3b shows RF using the extended RCP8.5 out to 2300. For CO_2, the percentage difference between RF values using old and new expressions increases to about 9%, illustrating the importance of the nonconstant a term. For N_2O and CH_4 RF, the difference between the new and old expressions in 2300 reaches −21% and 12%, respectively. Thus, in future scenarios the new expressions suggest that forcing will be even higher than current estimates due to the increase in CO_2 and CH_4 RF, which is slightly offset by the decrease in N_2O forcing, which is due to CO_2 overlap at high CO_2 concentrations.

The calculations of metrics (global warming potential (GWP) and global temperature change potential (GTP)) presented in *Myhre et al.* [2013a] are also impacted. These utilize radiative efficiencies (REs) for small perturbations around present-day concentrations. For CO_2 and N_2O these are affected by about 1% or less compared to the values presented in Table 8.A1 of *Myhre et al.* [2013a]. By contrast, the CH_4 radiative efficiency (RE), for small perturbations about present-day concentrations, increases from 3.63×10^{-4} to 4.48×10^{-4} W m^{-2} ppb^{-1}, an increase of 23%. This percentage difference is slightly lower than for the industrial era CH_4 change because differences in the updated expression relative to MHSS98 are largest for low CH_4 concentrations (see Table S1). Since the GWP and GTP values for CH_4 in *Myhre et al.* [2013a] include indirect effects due to ozone and stratospheric water vapor change, and the absolute contribution of these is unchanged by the increase in the RE, the metrics themselves

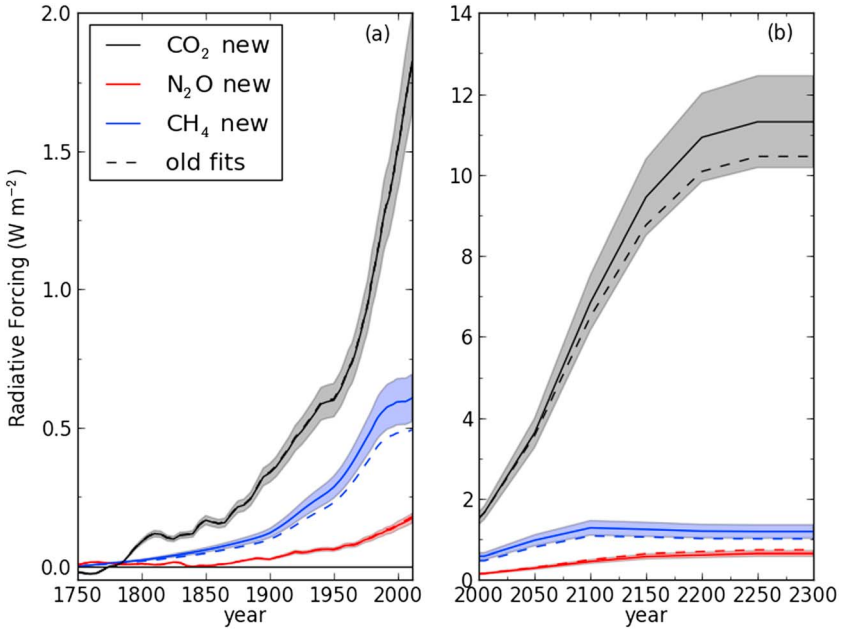

Figure 3. Radiative forcing of CO_2, N_2O, and CH_4 concentration change: (a) from 1755 to 2011 and (b) from 2000 to 2300 (using RCP8.5 concentrations from *Meinshausen et al.* [2011]) relative to preindustrial value (280 ppm of CO_2, 275 ppb of N_2O, and 750 ppb of CH_4) using old and new simplified expressions. Shading for the new expressions indicates the estimated radiative uncertainty in the forcing (see section 3.4).

increase by about 14%. The GWP for the 100 year time horizon, the most commonly used metric, increases from 28 to 32.

6. Conclusions

New line-by-line calculations of RF due to CO_2, CH_4, and N_2O are used as a basis to update the simple expressions in MHSS98 that have been used widely, including in IPCC assessments, to calculate WMGHG forcings. While the changes to CO_2 and N_2O RF between the old and new fits are within the 10% uncertainty estimate given in *Myhre et al.* [2013a], the changes in the CH_4 RF are significantly larger. We show that inclusion of the shortwave (near-infrared) bands of methane, which were neglected in many previous analyses, is most responsible for this change; there is a smaller contribution due to an update of the water vapor foreign continuum relative to that used in MHSS98. The new expressions reproduce the line-by-line calculations to better than 5%, but the quality of the fits must be distinguished from the uncertainty in the forcing calculations themselves—based on previous work and calculations performed here, we assess the uncertainty to be ±10% for CO_2 and N_2O and ±14% for CH_4. The higher uncertainty for CH_4 arises from the greater importance of the shortwave forcing. The results emphasize the need for continuing assessment and refinement of RF calculations used in deriving such simple expressions. Further assessment of the methane shortwave effect is particularly warranted, as is continued examination of the fundamental spectroscopic basis of greenhouse gas radiative forcing calculations [e.g., *Mlynczak et al.*, 2016].

Acknowledgments
K.P.S. acknowledges the UK Natural Environment Research Council research grant SMURPHS (NE/N006054/1) for support in the latter stages of this work. G.M. is supported by the Research Council of Norway project MOCA, grant 225814. We thank Eugene Rozanov for providing the detailed methane forcing results in the CCMval radiation code intercomparison, Glynn Heritage-Finney for exploratory calculations of the impact of N_2O-CO_2 overlaps which helped motivate part of this work, and Ramiro Checa-Garcia for comments. Reviewers' comments were particularly helpful. All data used in this study are available in the referenced papers.

References

Byrne, B., and C. Goldblatt (2014), Radiative forcing at high concentrations of well-mixed greenhouse gases, *Geophys. Res. Lett.*, *41*, 152–160, doi:10.1002/2013gl058456.

Collins, W. D., et al. (2006), Radiative forcing by well-mixed greenhouse gases: Estimates from climate models in the Intergovernmental Panel on Climate Change (IPCC) Fourth Assessment Report (AR4), *J. Geophys. Res.*, *111*, D14317, doi:10.1029/2005JD006713.

Fomichev, V., and P. M. Forster (2010), Radiation, in *SPARC Report on the Evaluation of Chemistry-Climate Models, SPARC Reports No 5, WCRP-132, WMO/TD-No. 152*, edited by V. Eyring, T. Shepherd, and D. Waugh, pp. 71–108, World Meteorological Organization.

Forster, P., et al. (2005), Resolution of the uncertainties in the radiative forcing of HFC-134a, *J. Quant. Spectrosc. Radiat. Transfer*, *93*(4), 447–460, doi:10.1016/j.jqsrt.2004.08.038.

Forster, P. M., et al. (2011), Evaluation of radiation scheme performance within chemistry climate models, *J. Geophys. Res.*, *116*, doi:10.1029/2010JD015361.

Hansen, J., M. Sato, R. Ruedy, A. Lacis, and V. Oinas (2000), Global warming in the twenty-first century: An alternative scenario, *Proc. Natl. Acad. Sci. U.S.A.*, *97*(18), 9875–9880, doi:10.1073/pnas.170278997.

Hansen, J., I. Fung, A. Lacis, D. Rind, S. Lebedeff, R. Ruedy, G. Russell, and P. Stone (1988), Global climate changes as forecast by Goddard Institute for Space Studies three-dimensional model, *J. Geophys. Res.*, *93*(D8), 9341–9364, doi:10.1029/JD093iD08p09341.

Haywood, J. M., and K. P. Shine (1997), Multi-spectral calculations of the direct radiative forcing of tropospheric sulphate and soot aerosols using a column model, *Q. J. R. Meteorol. Soc.*, *123*(543), 1907–1930, doi:10.1002/qj.49712354307.

Hodnebrog, Ø., M. Etminan, J. S. Fuglestvedt, G. Marston, G. Myhre, C. J. Nielsen, K. P. Shine, and T. J. Wallington (2013), Global warming potentials and radiative efficiencies of halocarbons and related compounds: A comprehensive review, *Rev. Geophys.*, *51*, 300–378, doi:10.1002/rog.20013.

Johansson, D. J. A., B. C. O'Neill, C. Tebaldi, and O. Haggstrom (2015), Equilibrium climate sensitivity in light of observations over the warming hiatus, *Nature Climate Change*, *5*(5), 449–453, doi:10.1038/nclimate2573.

Kratz, D. P. (2008), The sensitivity of radiative transfer calculations to the changes in the HITRAN database from 1982 to 2004, *J. Quant. Spectrosc. Radiat. Transfer*, *109*(6), 1060–1080, doi:10.1016/j.jqsrt.2007.10.010.

Lean, J., G. Rottman, J. Harder, and G. Kopp (2005), SORCE contributions to new understanding of global change and solar variability, *Sol. Phys.*, *230*(1–2), 27–53, doi:10.1007/s11207-005-1527-2.

Li, J., C. L. Curry, Z. Sun, and F. Zhang (2010), Overlap of solar and infrared spectra and the shortwave radiative effect of methane, *J. Atmos. Sci.*, *67*(7), 2372–2389, doi:10.1175/2010jas3282.1.

Masson-Delmotte, V., et al. (2013), Information from paleoclimate archives, in *Climate Change 2013: The Physical Science Basis. Contribution of Working Group I to the Fifth Assessment Report of the Intergovernmental Panel on Climate Change*, edited by T. F. Stocker et al., pp. 383–464, Cambridge Univ. Press, Cambridge, U. K., and New York.

Meinshausen, M., et al. (2011), The RCP greenhouse gas concentrations and their extensions from 1765 to 2300, *Climatic Change*, *109*(1–2), 213–241, doi:10.1007/s10584-011-0156-z.

Mlawer, E. J., S. A. Clough, P. D. Brown, and D. C. Tobin (1998), Collision-induced effects and the water vapor continuum, in *Eighth Atmospheric Radiation Measurement (ARM) Science Team Meeting*, edited, pp. 503–511, ARM, Tucson, Ariz.

Mlawer, E. J., V. H. Payne, J. L. Moncet, J. S. Delamere, M. J. Alvarado, and D. C. Tobin (2012), Development and recent evaluation of the MT_CKD model of continuum absorption, *Philosophical Transactions of the Royal Society a-Mathematical Physical and Engineering Sciences*, *370*(1968), 2520–2556, doi:10.1098/rsta.2011.0295.

Mlynczak, M. G., T. S. Daniels, D. P. Kratz, D. R. Feldman, W. D. Collins, E. J. Mlawer, M. J. Alvarado, J. E. Lawler, L. W. Anderson, and D. W. Fahey (2016), The spectroscopic foundation of radiative forcing of climate by carbon dioxide, *Geophys. Res. Lett.*, *43*, doi:10.1002/2016GL068837.

Myhre, G., E. Highwood, K. Shine, and F. Stordal (1998), New estimates of radiative forcing due to well mixed greenhouse gases, *Geophys. Res. Lett.*, *25*(14), 2715–2718, doi:10.1029/98GL01908.

Myhre, G., F. Stordal, I. Gausemel, C. J. Nielsen, and E. Mahieu (2006), Line-by-line calculations of thermal infrared radiation representative for global condition: CFC-12 as an example, *J. Quant. Spectrosc. Radiat. Transfer*, *97*, 317–331, doi:10.1016/j.jqsrt.2005.04.015.

Myhre, G., et al. (2009), Intercomparison of radiative forcing calculations of stratospheric water vapour and contrails, *Meteorologische Zeitschrift*, *18*(6), 585–596, doi:10.1127/0941-2948/2009/0411.

Myhre, G., et al. (2013a), Anthropogenic and natural radiative forcing, in *Climate Change 2013: The Physical Science Basis. Contribution of Working Group I to the Fifth Assessment Report of the Intergovernmental Panel on Climate Change*, edited by T. F. Stocker et al., pp. 659–740, Cambridge Univ. Press, Cambridge, U. K., and New York.

Myhre, G., et al. (2013b), Radiative forcing of the direct aerosol effect from AeroCom Phase II simulations, *Atmos. Chem. Phys.*, *13*, 1853–1877, doi:10.5194/acp-13-1853-2013.

Ramaswamy, V., O. Boucher, J. Haigh, D. Hauglustaine, J. Haywood, G. Myhre, T. Nakajima, G. Y. Shi, and S. Solomon (2001), Radiative forcing of climate change, in *Climate Change 2001: The Scientific Basis. Third Assessment Report of the Intergovernmental Panel on Climate Change*, edited by J. T. Houghton et al., pp. 349–416, Cambridge, Cambridge.

Randles, C. A., et al. (2013), Intercomparison of shortwave radiative transfer schemes in global aerosol modeling: Results from the AeroCom Radiative Transfer Experiment, *Atmos. Chem. Phys.*, *13*, 2347–2379, doi:10.5194/acp-13-2347-2013.

Rind, D., and A. Lacis (1993), The role of the stratosphere in climate change, *Surveys in Geophysics*, *14*(2), 133–165, doi:10.1007/bf02179221.

Rothman, L. S., et al. (2009), The HITRAN 2008 molecular spectroscopic database, *J. Quant. Spectrosc. Radiat. Transfer*, *110*(9–10), 533–572, doi:10.1016/j.jqsrt.2009.02.013.

Rothman, L. S., et al. (2013), The HITRAN2012 molecular spectroscopic database, *J. Quant. Spectrosc. Radiat. Transfer*, *130*, 4–50, doi:10.1016/j.jqsrt.2013.07.002.

Shi, G. Y. (1992), Radiative forcing and greenhouse effect due to atmospheric trace gases, *Science in China Series B-Chemistry*, *35*(2), 217–229.

Shine, K. P., R. G. Derwent, D. J. Wuebbles, and J.-J. Morcrette (1990), Radiative forcing of climate, in *Climate Change: The IPCC Scientific Assessment*, edited by J. T. Houghton, G. J. Jenkins, and J. J. Ephraums, pp. 41–68, Cambridge, Cambridge.

Shine, K. P., A. Campargue, D. Mondelain, R. A. McPheat, I. V. Ptashnik, and D. Weidmann (2016), The water vapour continuum in near-infrared windows—Current understanding and prospects for its inclusion in spectroscopic databases, *J. Mol. Spectrosc.*, *327*, 193–208, doi:10.1016/j.jms.2016.04.011.

Skeie, R. B., T. Berntsen, M. Aldrin, M. Holden, and G. Myhre (2014), A lower and more constrained estimate of climate sensitivity using updated observations and detailed radiative forcing time series, *Earth System Dynamics*, *5*(1), 139–175, doi:10.5194/esd-5-139-2014.

Stamnes, K., S. C. Tsay, W. Wiscombe, and K. Jayaweera (1988), Numerically stable algorithm for discrete-ordinate-method radiative transfer in multiple-scattering and emitting layered media, *Appl. Opt.*, *27*(12), 2502–2509.

Toon, G. C., J. F. Blavier, K. Sung, L. S. Rothman, and I. E. Gordon (2016), HITRAN spectroscopy evaluation using solar occultation FTIR spectra, *J. Quant. Spectrosc. Radiat. Transfer*, *182*, 324–336, doi:10.1016/j.jqsrt.2016.05.021.

Wigley, T. M. L. (1987), Relative contributions of different trace gases to the greenhouse effect, *Climate Monitor*, *16*, 14–29.

Zhong, W. Y., and J. D. Haigh (2013), The greenhouse effect and carbon dioxide, *Weather*, *68*(4), 100–105, doi:10.1002/wea.2072.